1 **Transported African Dust in the Lower Marine Atmospheric Boundary Layer is Internally**

2 **Mixed with Sea Salt Contributing to Increased Hygroscopicity and a Lower Lidar**

3 **Depolarization Ratio**

4 Sujan Shrestha[1], Robert E. Holz[2*], Willem J. Marais[2], Zachary Buckholtz[2], Ilya Razenkov[2],

5 Edwin Eloranta[2], Jeffrey S. Reid[3], Hope E. Elliott[1,a], Nurun Nahar Lata[4], Zezhen Cheng[4], Swarup

6 China[4], Edmund Blades[1], Albert D. Ortiz[1], Rebecca Chewitt-Lucas[5], Alyson Allen[1], Devon

7 Blades[1], Ria Agrawal[1], Elizabeth A. Reid[3], Jesus Ruiz-Plancarte[6], Anthony Bucholtz[6], Ryan

8 Yamaguchi[6], Qing Wang[6], Thomas Eck[7], Elena Lind[7], Mira L. Pöhlker[8], Andrew P. Ault[9],

9 Cassandra J. Gaston[1*]

10 [1]Department of Atmospheric Sciences, Rosenstiel School of Marine, Atmospheric, and Earth
11 Science, University of Miami, FL, USA

12 [2]Space Science and Engineering Center (SSEC), University of Wisconsin-Madison, WI, USA

13 [3]U.S. Naval Research Laboratory, Monterey, CA, USA

14 [4]Environmental Molecular Sciences Laboratory, Pacific Northwest National Laboratory,
15 Richland, WA, USA

16 [5]Caribbean Institute for Meteorology and Hydrology, Barbados

17 [6]Department of Meteorology, Naval Postgraduate School, Monterey, CA, USA

18 [7]NASA Goddard Space Flight Center, Greenbelt, MD, USA

19 [8]Atmospheric Microphysics Department, Leibniz Institute for Tropospheric Research, Leipzig,
20 Germany

21 [9]Department of Chemistry, University of Michigan, MI, USA

22 [a]now at Department of Biological & Environmental Sciences, Wittenberg University, Springfield,
23 OH, USA

24 *Corresponding Author: Cassandra J. Gaston: Email: cgaston@miami.edu, Phone: (305)-421-
25 4979 and Robert E. Holz: Email: reholz@ssec.wisc.edu

Abstract

Saharan dust is frequently transported across the Atlantic, yet the chemical, physical, and morphological transformations dust undergoes within the marine atmospheric boundary layer (MABL) remain poorly understood. These transformations are critical for understanding dust's radiative and geochemical impacts, it's representation in atmospheric models, and detection via remote sensing. Here, we present coordinated observations from the Office of Naval Research's Moisture and Aerosol Gradients/Physics of Inversion Evolution (MAGPIE) August 2023 campaign at Ragged Point, Barbados. These include vertically resolved single-particle analyses, mass concentrations of dust and sea spray, and High Spectral Resolution Lidar (HSRL) retrievals. Single-particle data show that dust within the Saharan Air Layer (SAL) remains externally mixed, with a corresponding high HSRL-derived linear depolarization ratio (LDR) at 532 nm of ~0.3. However, at lower altitudes, dust becomes internally mixed with sea spray, and under the high humidity (>80%) of the MABL undergoes hygroscopic growth, yielding more spherical particles, suppressing the LDR to <0.1; even in the presence of high dust loadings (e.g., ~120 $\mu g/m^3$). This low depolarization in the MABL is likely due to a combination of the differences between the single scattering properties of dust and spherical particles, and the potential modification of the dust optical properties from an increased hygroscopicity of dust caused by the mixing with sea salt in the humid MABL. These results highlight the importance of the aerosol particle mixing state when interpreting LDR-derived dust retrievals and estimating surface dust concentrations in satellite products and atmospheric models.

1. Introduction

The transport of Saharan dust across the North Atlantic Basin throughout the year is one of the largest aerosol phenomena observable from space. The most intensive events often occur during the boreal summer when large quantities of dust are lofted and advected westward by trade winds within the Saharan Air Layer (SAL), a well-defined elevated layer extending from ~2 to 5 km above mean sea level (AMSL) (e.g., Carlson and Prospero, 1972; Karyampudi et al., 1999; Adams et al., 2012; Tsamalis et al., 2013; Mehra et al., 2023). This conceptual model of African dust transport is frequently reinforced by satellite and ground-based remote sensing, particularly lidar (Burton et al., 2012, 2015), multi-angle imager (Kalashnikova et al., 2013), polarimetric (Huang et al., 2015) or combination of these observations (Moustaka et al., 2025) that rely on dust's asphericity to differentiate coarse mode dust from other aerosol sources such as hydrated sea spray. These techniques often detect little dust within the lower marine atmospheric boundary layer (MABL). However, it is well known that exceptionally high dust concentrations are often directly measured in the MABL (e.g., Reid et al., 2003b; Zuidema et al., 2019; Elliott et al., 2024; Mayol-Bracero et al., 2025) and these layers are regularly forecast by operational dust transport models (Xian et al., 2019). This contradiction between the common conceptual model fueled by remote sensing of elevated dust layers versus evidence of significant near-surface dust mass concentrations by in situ observations raises a critical question, is there an observational gap in the detection and characterization of dust within the MABL?

Among the methods to speciate airborne dust from other aerosol particle types, the most common benchmark is to rely on dust's asphericity, and its impact on lidar's linear depolarization ratio (LDR). The LDR is based on a lidar's range-resolved measurement of the fraction of backscattered light by aerosol particles that become depolarized from the original polarized laser

69   pulse. Backscattered light from homogeneous spherical particles, such as hydrated sea salt, has

70   low depolarization (e.g., LDR remains minimal) whereas particles with asymmetry such as dry,

71   irregular dust will return a partially depolarized signal, typically ~0.25-0.40 (Murayama et al.,

72   1999; Ansmann et al., 2012; Burton et al., 2012; Freudenthaler et al., 2009; Sakai et al., 2010;

73   Groß et al., 2016).

74   The assertion that dust can be isolated from other aerosol types such as in the references

75   above is well supported by both theoretical foundations and numerous observations of elevated

76   dust plumes. An important assumption in the detection of dust via the LDR is that the dust is not

77   hygroscopic. In situ observations of dust hygroscopicity in the MABL, typically using the

78   standard technique of drying and subsequently rehydrating particles ahead of nephelometer

79   measurements (Orozco et al., 2016), have suggested MABL dust is not significantly hygroscopic

80   (Li-Jones et al., 1998; Zhang et al., 2014). Thus, it is often assumed that dust in the humid

81   MABL will retain its aspherical shape and remain tracible via the LDR. However, even freshly

82   emitted dust or that which is sampled well within a dust plume can contain soluble minerals that

83   should be inherently hygroscopic and could affect detection of dust via the LDR (Koehler et al.,

84   2007; Reid et al., 2003a).

85   Contradictory observations have introduced uncertainty in the interpretation of lidar

86   observations for dust detection in the MABL. For example, during the SALTRACE campaign in

87   Barbados, lidar-derived LDR measurements within the lower MABL were 0.15 ± 0.02,

88   suggesting approximately equal parts spherical and non-spherical particles, despite in-situ

89   observations indicating surface dust mass concentrations as high as 40 $\mu g/m^3$ (Groß et al., 2016;

90   Weinzierl et al., 2017). Groß et al. (2016) also reported that dust mass concentrations exceeding

91   40 $\mu g/m^3$ could be underestimated by up to 50% by lidar-derived depolarization measurements,

92 in part due to the dominant influence of sea spray in the MABL that introduces large

93 concentrations of hydrated, spherical particles that reduce the overall depolarization signal.

94 Tsamalis et al. (2013) emphasized that the polluted dust aerosol type is often misclassified or

95 detected less often in spaceborne CALIOP observations due to low depolarization signals

96 resulting from dust mixing with other aerosol types such as biomass burning, marine or

97 anthropogenic aerosols (Yang et al., 2022; Kong et al., 2022). The relationship between dust

98 mass and depolarization has important implications for how the depolarization ratio is used to

99 infer surface-level dust concentrations in air quality forecasts and climate models. Since satellite

100 retrievals and column-integrated techniques lack vertical resolution, they may fail to capture

101 such near-surface morphological changes in dust (Li et al., 2020). If depolarization-based

102 methods underestimate dust presence near the surface under marine conditions, it could

103 introduce systematic errors in dust-related radiative forcing and deposition estimates. A similar

104 concern exists for multi-angle imagers and polarimetric retrievals that depend on assumptions of

105 particle asymmetry to detect and quantify dust.

106 During August 2023, the Office of Naval Research (ONR) initiated the Moisture and

107 Aerosol Gradients/Physics of Inversion Evolution (MAGPIE) field campaign at the University of

108 Miami's Barbados Atmospheric Chemistry Observatory (BACO) at Ragged Point, Barbados to

109 map the inhomogeneity of the MABL. Central to MAGPIE are studies to identify information

110 lost when one conceptualizes the MABL as a series of uniform layers (e.g., surface layer, mixed

111 layer, entrainment or detrainment zones, etc.). While MAGPIE's core objectives focus on

112 atmospheric flows and fluxes with an emphasis on active remote sensing, aerosol particles and

113 their optical closure were implicitly a core mission element because light scattering by these

114 particles can be used to track atmospheric motion. MAGPIE collaborated across U.S. federal

115   agencies, academic institutions, and the Caribbean Institute for Meteorology and Hydrology

116   (CIMH) and included observations from ground-based aerosol particle samplers and instruments

117   at BACO along with local flights from the Naval Postgraduate School (NPS) CIRPAS Twin Otter

118   (CTO) aircraft. Central to the mission was the University of Wisconsin Space Sciences and

119   Engineering Center's (SSEC) High Spectral Resolution Lidar (HSRL; Eloranta et al., 2008).

120   Here, single particle and bulk analyses are used to evaluate how measured dust and sea salt mass

121   concentrations relate to HSRL-derived particulate LDR. In Section 2, we provide a brief

122   overview of measurements, and in Section 3.1 a timeseries analysis of particle and lidar data,

123   demonstrating nonlinearity between dust and sea salt mass ratios to lidar LDR. In Sections 3.2

124   and 3.3, we provide vertically resolved single particle data from the CTO aircraft and ground-

125   based samples, respectively, to help explain the anomalies. In Section 4, we provide a discussion

126   and study conclusions.

127   **2.   Methods and materials**

128   **2.1. Sampling Site and Campaign Overview**

129   Ground-based aerosol particle and lidar measurements were conducted at the BACO site

130   on Ragged Point (13°6′N, 59°37′W) for August 2023. Situated at the easternmost point of the

131   Caribbean, BACO offers an optimal location for intercepting long-range transported Saharan

132   dust with minimal interference from local, anthropogenic emissions due to the prevalent Easterly

133   trade winds (Prospero et al., 2021; Gaston et al., 2024; Zuidema et al., 2019). Continuous aerosol

134   particle measurements have been conducted there for over 50 years, providing a unique long-

135   term observational record. The site is equipped with a tower that is 17 m high and is placed atop

136   a 30 m high bluff giving an altitude of ~50 m above sea level. While the measurements are not

137   taken directly at ground level, they are representative of the near surface MABL and are

138　routinely referred to as surface observations in prior Barbados studies (e.g., Zuidema et al.,

139　2019).

140　　　　MAGPIE leveraged multi-platform measurements including aerosol particles collected at

141　the top of the BACO sampling tower and aboard the CTO aircraft to investigate vertical

142　gradients in aerosol particle chemical and morphological properties. For the 2023 campaign, the

143　focus is centered around the largest dust events of the year observed between August 11-18,

144　2023. A total of five research flights were conducted during this period, with two samples

145　collected per flight, resulting in ten samples covering a range of altitudes from 30 m to 3 km

146　AMSL.

2.2. Dust Mass Concentration Measurement

148　　　　Aerosol particles were collected on top of the BACO tower using high-volume samplers

149　with Total Suspended Particulate (TSP) inlets and fitted with cellulose filters (Whatman-41, 20

150　µm pore size) with a particle size cutoff at 80-100 µm in diameter due to the geometry of the

151　rainhat as described in Royer et al. (2023). Procedural filter blanks were collected every five

152　days and processed alongside the daily filter samples. A quarter of each filter was sequentially

153　extracted three times using a total of 20 mL of Milli-Q water to remove soluble components.

154　Following extraction, the filters were combusted at 500 °C overnight in a muffle furnace. The

155　residual ash mass was weighed and corrected for background contributions by subtracting the

156　ash mass obtained from the procedural blank. The net ash mass was multiplied by a correction

157　factor of 1.3 to account for the loss of any soluble or volatile components during the extraction

158　and combustion process (Prospero, 1999; Zuidema et al., 2019). While some soluble components

159　such as halite may be lost during the extraction process, the applied correction factor of 1.3 is

160　intended to conservatively account for these potential losses, supporting more robust dust mass

161 estimates. Moreover, halite is not a major constituent of Saharan dust, as previous studies report

162 its contribution rarely exceeds 3% by weight (Scheuvens et al., 2013), making any bias from its

163 loss during the extraction process unlikely to be significant.

164 **2.3. Sea Salt Concentration Measurement**

165 The filtrate collected after dust extraction on the daily filter samples and procedural

166 blanks was then analyzed using ion chromatography (IC; Dionex Integrion HPIC System;

167 Thermo Scientific). The samples were analyzed in triplicate for cations and anions and corrected

168 for procedural blanks. Details of our IC analysis procedure can be found in Royer et al. (2025).

169 Sodium (Na^+) is commonly used as a conservative tracer for sea spray particles, therefore, the

170 Na^+ concentrations measured by IC analysis were converted to equivalent sea salt concentrations

171 by applying a multiplication factor of 3.252 (Eqn. 1) (Gaston et al, 2024; Prospero, 1979).

172 $$\text{Sea salt concentration} = [Na^+] * 3.252 \qquad \text{Eqn. 1}$$

173 **2.4. In-situ Ground-based Aerosol Optical Measurement**

174 BACO is part of NASA's AErosol RObotic NETwork (AERONET). We used AERONET

175 level 2 aerosol optical depth (AOD at 500 nm) and fine mode AOD (at 500 nm) from the

176 AERONET spectral deconvolution retrieval (O'Neill et al., 2003) to identify the times of dust

177 intrusion during the sampling campaign (Giles et al., 2019; Holben et al., 1998).

178 **2.5. Single-Particle Analysis and Mixing State**

179 Aerosol particle mixing state describes how chemical species are distributed across the

180 particle population (Winkler, 1973; Riemer et al., 2019). Single-particle analysis offers a

181 powerful approach for analyzing this complexity, providing direct insight into the internal

182 composition and variability of individual particles (Reid et al., 2003a; Ault et al., 2014, 2012;

183   Royer et al., 2023; Casuccio et al., 1983; Kim et al., 1987; Andreae et al., 1986; Zhang et al.,

184   2003; Levin et al., 2005; Kandler et al., 2018). We used computer-controlled scanning electron

185   microscopy (SEM, Quanta from Thermo Fisher Scientific, equipped with a FEI Quanta digital

186   field emission gun at 20 kV and 480 pA electron current) coupled with energy-dispersive X-ray

187   spectroscopy (EDX, Oxford UltimMax100) (CCSEM/EDX) at the Environmental Molecular

188   Sciences Laboratory (EMSL) located at the Pacific Northwest National Laboratory (PNNL) to

189   characterize single particles. EDX spectra are collected for semi-quantitative analysis of the

190   particle elemental composition, and our analysis focused on 16 elements commonly found in

191   atmospheric aerosol particles: carbon (C), nitrogen (N), oxygen (O), sodium (Na), magnesium

192   (Mg), aluminum (Al), silicon (Si), phosphorous (P), sulfur (S), chlorine (Cl), potassium (K),

193   calcium (Ca), vanadium (V), manganese (Mn), iron (Fe), and nickel (Ni). This analysis was

194   conducted for particles collected on the BACO tower and aboard the CTO aircraft.

195   2.5.1.   **Ground-based Particulate Samples for Single Particle Analysis**

196   Ambient aerosol particles were sampled on top of BACO's 17 m tower using a three-stage

197   cascade impactor (Microanalysis Particle Sampler, MPS-3; California Measurements, Inc.), that

198   separates particles into aerodynamic diameter ranges of 2.5-5.0 µm (stage 1), 0.7-2.5 µm (stage

199   2), and 0.05-0.7 µm (stage 3). Samples were collected for 30 minutes at 2 L/min each day.

200   Particles were deposited onto carbon-coated copper grids (Ted Pella, Inc.) and analyzed using

201   CCSEM/EDX. No conductive coating (e.g., gold or carbon) was applied to the samples collected

202   on the ground as the conductivity of the copper grid bars minimized possible impacts from

203   charging effects. However, Cu signals from CCSEM/EDX were excluded due to interference

204   from the substrate. In contrast, C films are thin and highly transparent to electrons. Although C

205   signals are present in all spectra due to the support film, the C layer is fine-grained and

206 minimally interferes with particle morphology. Moreover, C together with O, serves as a useful

207 qualitative indicator for identifying organic particles, defined by a combined C + O contribution

208 exceeding 95 %. In this study, N was not used for quantification, nor did we label it in the EDX

209 spectra of particles. Elemental signals were considered valid for further analysis only when

210 exceeding a 2% threshold composition detected by EDX spectra. Over 1,000 individual particles

211 were analyzed per sample. Post-processing of CCSEM/EDX data was conducted using a k-

212 means clustering algorithm (Ault et al., 2012; Shen et al., 2016; Royer et al., 2023) to group

213 particles by similarity in composition and morphology. Clusters were classified into particle

214 types primarily based on semiquantitative elemental composition obtained from EDX analysis,

215 supported by particle size, morphology, and comparison with prior studies. Mineral dust particles

216 were identified by the presence of aluminosilicate elements (Si, Al, and Fe) characteristic of

217 crustal minerals (Hand et al., 2010; Krueger et al., 2004; Levin et al., 2005; Krejci et al., 2005;

218 Denjean et al., 2015). Fe was detected in ~80 % of mineral dust particles at relative area

219 abundances of 10-15 %. Sea spray particles were characterized by strong Na and Cl peaks,

220 indicative of halite (NaCl) and confirming their marine origin (Bondy et al., 2018). Aged sea

221 spray particles were identified by Cl depletion accompanied by enrichment in S, consistent with

222 heterogeneous reactions that replace Cl with sulfate or nitrate (Ault et al., 2014; Royer et al.,

223 2023, 2025). Mineral dust particles were observed to be both internally mixed with sea spray and

224 externally mixed (Royer et al., 2023, 2025; Kandler et al., 2018; Harrison et al., 2022; Aryasree

225 et al., 2024). These internally mixed dust and sea spray particles exhibited heterogeneous

226 compositions containing both dust-derived (Si, Al, Fe, Mg) and marine-derived (Na, Cl, Mg)

227 components, with Mg potentially originating from both sources. Organic particles were

228 dominated by C and O (>95 %), with minor inorganic elements, and typically appeared as

229 spherical or gel-like structures. Some displayed Mg-rich shells with sea salt cores, consistent

230 with primary marine organics formed via bubble-bursting at the ocean surface (Ault et al., 2013;

231 Gaston et al., 2011; Chin et al., 1998). Sulfate-rich particles exhibited strong sulfur peaks with

232 accompanying C and O signals, indicative of marine secondary aerosols (e.g., ammonium sulfate

233 or bisulfate) and frequently contained an organic fraction (O'Dowd and de Leeuw, 2007; Royer

234 et al., 2023).

235 2.5.2. **Airborne Particulate Samples for Single Particle Analysis**

236 Aerosol samples were also collected onboard the CTO using an isokinetic inlet and deposited

237 onto isopore membrane filters (47 mm filter, 0.8 µm pore size). An overview of the airborne

238 sampling technique can be found in the Supporting Information (SI Text S1). The CTO's primary

239 inlet has an intrinsic 50 % cutpoint of ~3.5 µm in aerodynamic diameter. Due to limitations

240 associated with Teflon filter material, automated computer-controlled SEM was not feasible, and

241 these airborne samples were analyzed manually using SEM/EDX. To prevent particle charging

242 during imaging, filters were sputtered with a gold-coating of 10 nm thickness prior to analysis. A

243 total of 40, 21, and 52 particles from 250 nm to 25 µm diameter were manually analyzed from

244 samples collected within the SAL, above, and below cloud base heights (CBH), respectively,

245 providing a primarily qualitative assessment. The CBH was identified for each flight as the first

246 maximum in profile relative humidity, typically near saturation. Details of airborne sample

247 collection date and times, durations, altitudes, and corresponding CBH are provided in Table S1.

248 Particles were selected randomly across the filter area without targeting specific particle types or

249 sizes to reduce selection bias. All filter handling was performed in a laminar flow hood, and

250 filters were stored individually in sealed Teflon-taped Petri dishes to avoid any contamination.

251 The number of particles analyzed is reported in Table S2 of the SI. To quantify statistical

252 uncertainty, we calculated 95% confidence intervals for the number fraction of each particle class

253 assuming binomial sampling. The major particle types show varying levels of statistical

254 precision. For example, mineral dust is clearly dominant in the SAL (90 ± 9 %) and statistically

255 distinct from mixed dust and sea spray particles, whereas above cloud top and below cloud base,

256 mineral dust and internally mixed dust and sea spray fractions have overlapping confidence

257 intervals, indicating comparable abundance within uncertainty. Thus, while the data robustly

258 supports dust dominance in the SAL, compositional differences among dust and dust mixed with

259 sea spray particle types in the above cloud top and below cloud base should be interpreted

260 qualitatively. Whenever possible, ground-based measurements were coordinated to coincide with

261 periods when the CTO aircraft intercepted the BACO location or its vicinity. Single particle

262 analysis from aircraft sampling, presented in Section 3.2, serves as a comparative reference to

263 the more comprehensive in-situ ground-based dataset, which includes ~24,000 analyzed

264 particles. The sulfate and organic particle types were absent in the airborne samples. This is

265 likely due, in part, to the use of isopore filters with a relatively large pore size (0.8 µm), that may

266 have limited the collection efficiency of finer sulfate and organic rich particles.

267 **2.6. High Spectral Resolution Lidar (HSRL)**

268   The SSEC HSRL was deployed during the summer 2023 MAGPIE campaign to

269 characterize the vertical distribution of aerosol particle scattering properties over Ragged Point.

270 The HSRL system used in this study can provide range-resolved profiles of particulate

271 backscatter and depolarization at high spatial and temporal resolution. Details on the SSEC

272 HSRL can be found elsewhere (Razenkov, 2010; Eloranta et al., 2008; Reid et al., 2025). Briefly,

273 the SSEC HSRL operates at a wavelength of 532 nm and separates molecular and particulate

274 backscatter signals using a narrowband iodine absorption filter. This configuration enables

275   accurate, independent retrievals of particulate backscatter ($m^{-1}\ sr^{-1}$) within close proximity to the

276   ocean surface, as well as calibrated extinction (m^{-1}) and extinction-to-backscatter ratio (i.e., the

277   lidar ratio) measurements. The HSRL also contains an elastic backscatter channel of 1064 nm.

278   Long term Raman lidar measurements from the Max Planck Institute (MPI) in Barbados

279   (Weinzierl et al., 2017; Groß et al., 2015; Stevens et al., 2016) provides historical context for

280   aerosol backscatter and depolarization over the island and show structures consistent with the

281   HSRL observations presented here.

282   For MAGPIE, the SSEC-HSRL was configured to operate in periods of vertical stare,

283   horizontal stare, and vertical scanning from -0.05º to 18º. For the purposes of this paper, we only

284   utilize vertical data. Extraction of light extinction and the lidar ratio within the MABL are

285   performed using the HSRL in one of its side or vertically scanning modes. While a manuscript is

286   under preparation (Fu et al., 2025, in prep.), for the purpose of this paper we can report from its

287   authors that lidar ratios in the MABL's mixed layer ranged from 15 to 25 sr, and in the SAL was

288   on the order of 35-40 sr. Lidar ratios of 15-20 sr are consistent with ambient sea salt (RH= 70-

289   85% near the surface) and 40 sr above the MABL for "dry" dust in the less humid SAL (RH= 30-

290   50%).

291   **3. Results and discussion**

292   **3.1. Temporal variability in surface-level aerosol particle chemistry, AOD and lidar**

293   **depolarization ratios (LDR) during a major dust event**

294   Figure 1 presents a time series of key aerosol properties observed during the August 2023

295   MAGPIE intensive operations period, including surface-level dust and sea salt mass

296   concentrations, aerosol optical depth (AOD), and HSRL-derived particulate linear depolarization

297   ratio (LDR) and particulate backscatter. Over the month, median dust and sea salt concentrations

298   were 6 ± 32 and 17 ± 9 µg/m^3, respectively; the median columnar AOD was 0.15 ± 0.19; and the

299   median LDR at 135 m AMSL was 0.02 ± 0.03. Notably, a distinct deviation from these baseline

300   values was observed during a period of Saharan dust intrusion occurring between August 11 and

301   18, 2023. The dust event led to pronounced changes in the chemical composition and physical

302   properties of aerosol particles observed in Barbados, yet the LDR showed little increase. During

303   this period, the dust mass concentration peaked at 120 µg/m^3 on August 15, comparable to the

304   concentration measured during the major "Godzilla" dust event of 2020 (Elliott et al., 2024;

305   Mayol-Bracero et al., 2025), while inferred sea salt concentrations based on sodium were 27

306   µg/m^3, representing an upper-limit estimate given the possible contribution of Na from mineral

307   dust. The average dust-to-sea salt mass ratio was ~3.4 on dusty days (peaking at 4.8), compared

308   to ~0.40 on non-dusty days, indicating a clear dominance of dust in the lower MABL during the

309   dust intrusion event. Total column AOD (550 nm) closely tracked the trend in surface dust mass

310   concentration and peaked at ~0.75 on August 15, whereas fine mode AOD remained

311   substantially lower (0.12 ± 0.01; Fig. 1b) indicating that the total AOD was predominantly

312   influenced by coarse-mode particles during the dust period. Notably, this event produced one of

313   the highest AOD recorded in Barbados during the month of August over the past decade (Fig.

314   S1).

315
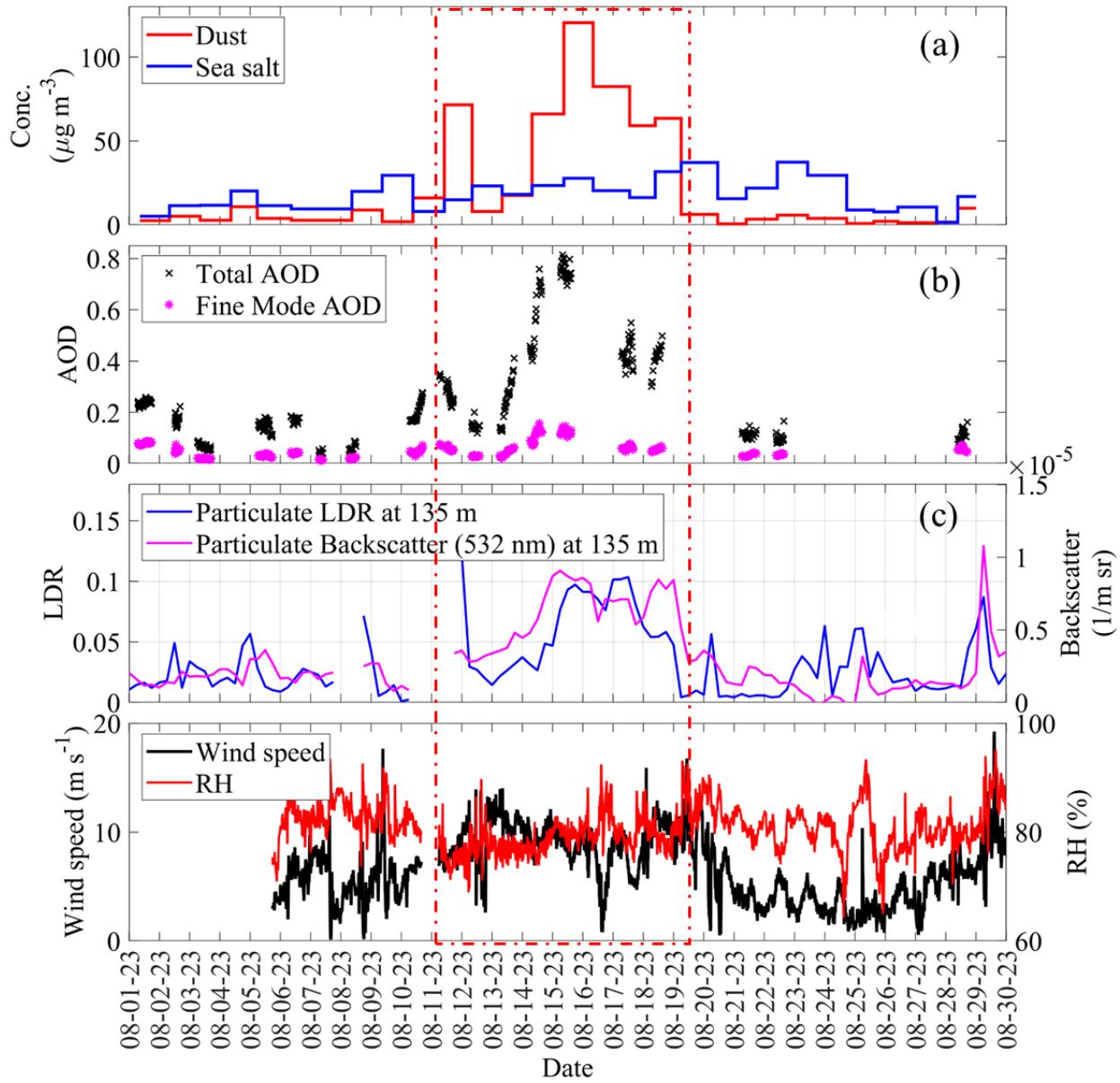
Figure 1. Time series plots for (a) dust and sea salt mass concentrations measured from the top of the BACO tower, (b) AERONET total column and fine mode fraction AODs (at 500 nm), (c) HSRL- particulate linear depolarization ratio (LDR) and particulate backscatter at 532 nm, averaged over six hours, and (d) meteorological measurements (RH and wind speed) during the MAGPIE 2023 campaign. The red dashed box represents the major dust intrusion periods observed during the campaign.

322   Figure 1c presents the time series of the particulate backscatter and LDR at 135 m

323   AMSL, representing conditions near the surface within the lower MABL for comparison with

324   other ground-based measurements. Although an increase in LDR was observed in the lower

325   MABL during the period of pronounced dust loading, the enhancement was surprisingly small,

326   with values of 0.10 or less (Fig. 1c). The finding can be partially explained through scattering

327   physics (e.g., the lidar equation) governing the lidar signals (Hayman and Spuler, 2017). For

328   MAGPIE, the HSRL lidar ratio (LR), the ratio of aerosol extinction (m^{-1}) to backscatter (m^{-1} sr$^-$

329   ^{1}), was approximately 40 sr for dust and 20 sr for marine aerosols. Because LR is inversely

330   related to the particulate 180° backscatter phase function, a lower LR indicates that marine

331   aerosol particles scatter back approximately twice the amount of energy compared to dust if the

332   marine and dust extinctions are the same. This difference in backscatter directly affects the

333   measured LDR. In a mixed aerosol layer with comparable extinction from dust and marine

334   particles, the backscattered signal, on which the LDR is based, is weighed more strongly toward

335   the marine aerosol contribution (that has a lower LDR).

336   Given that dust concentrations were approximately four times greater than those of sea

337   salt during the peak of the event, we applied a multiple regression approach to estimate the LDR,

338   using Eqn. 2, that incorporated the measured lidar ratio and dust and sea salt concentrations.

339    $$LDRexpected = \frac{v_{\perp}^{(d)}}{v_{\parallel}^{(d)} + v_{\parallel}^{(m)}} + \frac{v_{\perp}^{(m)}}{v_{\parallel}^{(d)} + v_{\parallel}^{(m)}} \qquad Eqn.\,2$$

340   where, $v_{\parallel}^{(d)}$ and $v_{\parallel}^{(m)}$ represent the parallel components, and $v_{\perp}^{(d)}$ and $v_{\perp}^{(m)}$ represent the

341   perpendicular components of the particulate backscatter from dust ("d") and marine aerosol

342   ("m") particles, respectively.

343   This analysis yielded an estimated LDR of 0.17 ± 0.03 during the dust peak, ~2 times higher

344   than the values observed in Fig 1c in the lower MABL. Details about this calculation and

345   approximations used to derive this estimate are in SI Text S3. Figure 2 shows the relationship

346   between the dust-to-sea salt mass concentration ratio versus the measured HSRL-derived LDR

347   and estimated LDR from the multiple regression approach. We note several caveats to our

348   calculation of the estimated LDR. First, the uncertainty associated with our estimated LDR

349   prediction may be larger than the standard deviation reported, as we did not explicitly account

350   for the full-size distribution of sea salt and dust aerosols. In particular, large particles beyond the

351   upper cut point (>80 -100 μm) of our bulk dust sampler were not captured. While previous

352   studies have shown that some particles of this size can survive trans-Atlantic transport (e.g.,

353   Betzer et al., 1988; Reid et al., 2003a; Barkley et al., 2021), their number concentrations are

354   expected to be substantially lower than those of the particle sizes efficiently collected by the

355   filter sampling used in this study. These coarse particles, which are more efficient at depolarizing

356   incident light due to their irregular shape and size, could contribute significantly to the lidar

357   signal. Their absence from the analysis may lead to an underestimation of the true depolarization

358   potential, especially during intense dust events. Nevertheless, we recognize that other factors

359   may also influence the observed reduction in depolarization. Vertical heterogeneity within the

360   MABL, including overlapping layers of marine and dust aerosols, could further convolute the

361   dust depolarization signal. In addition, inherent limitations in HSRL retrievals, such as signal

362   averaging in optically thin layers or reduced sensitivity near the ocean surface may contribute to

363   the apparent underestimation of LDR.

364
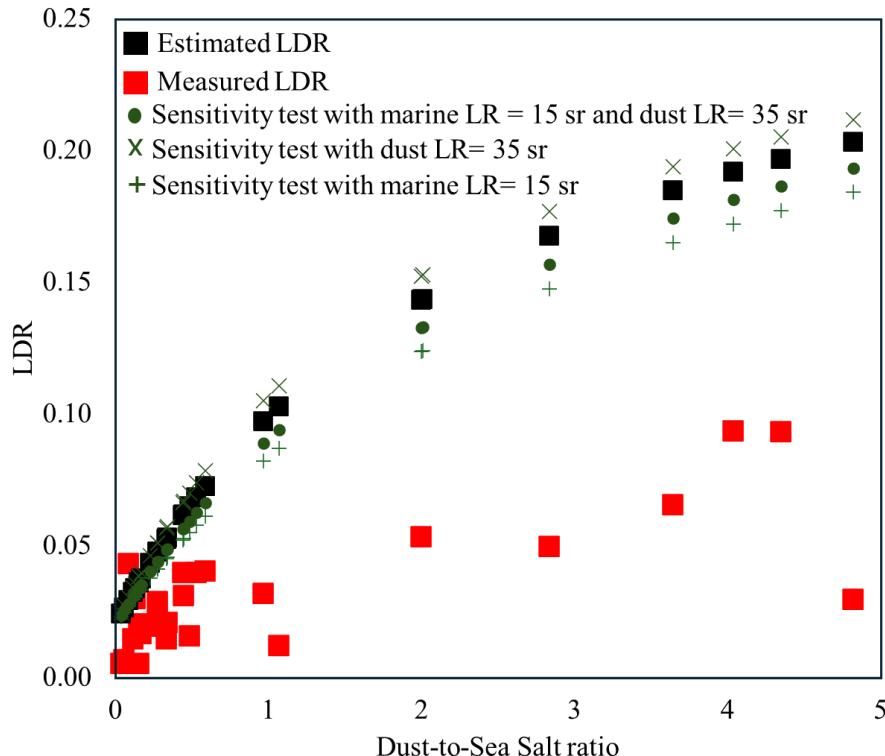
Figure 2. Relationship between the dust-to-sea salt concentration ratio and HSRL-derived

particulate LDR at 135 m above ground level during the MAGPIE campaign. Red squares

indicate measured LDR values for the full campaign, while black squares represent LDR values

estimated from mass concentrations and lidar ratio weighting during the peak dust event. The

calculated LDR was approximately a factor of two higher than what was observed during the

peak dust event. A sensitivity test was conducted using more conservative lidar ratio values for

dust and marine aerosols (shown as green plus, cross and circle symbols), and in all such cases

the estimated LDR values remained consistently higher than the measured values.

Extending our findings in Figure 1c vertically, Figure 3a and b shows the time series of

particulate backscatter and LDR measurements from August 12-18, 2023, at altitude up to 6 km

AMSL. At ~2-6 km AMSL above Ragged Point, measurements of increased particulate

backscatter (shown in Fig 3a) are primarily attributable to increased dust loading within the SAL,

18

377 as indicated by the concurrent elevated LDR of 0.30 (shown in Fig 3b). This altitude range is

378 consistent with previous studies that have reported the SAL to typically extend from

379 approximately 1.5 to 5.5 km AMSL (Carlson and Prospero, 1972; Groß et al., 2015; Karyampudi

380 and Carlson, 1988; Reid et al., 2003; Weinzierl et al., 2017). The particulate backscatter

381 measurement shown in Fig. 3a highlights high aerosol loading near the surface, consistent with

382 the large concentration of marine particles in the lower MABL. Notably, periods of enhanced

383 backscatter between August 14-16 extending downward from the SAL into the MABL suggest

384 episodes of dust downmixing toward the surface, which are also supported by a concurrent

385 increase in surface dust mass concentrations (Fig. 1).

386   Figure 3c shows the representative vertical distribution of RH during the dusty period of

387 the study, revealing a distinctly moist MABL characterized by RH values exceeding 80%. Such

388 elevated humidity levels are conducive to the hygroscopic growth of aerosol particles, which can

389 increase both particle size and sphericity (Titos et al., 2016). These changes in particle properties

390 caused by hygroscopic growth can further enhance particle backscatter while decreasing the

391 LDR which is visible in the particulate backscatter (Fig. 3a) and LDR (Fig. 3b) measurements

392 below cloud base (~700 m). Thus, under humid MABL conditions, both the LR contrast between

393 dust and marine aerosols and hygroscopicity-driven growth can act together to suppress the

394 observed LDR. However, a key consideration is aerosol mixing state as previous observations

395 have shown limited hygroscopic growth of African dust particles, even at high RH, but

396 substantial growth of dust particles that are internally mixed with other aerosol components

397 including sea spray (Denjean et al., 2015).
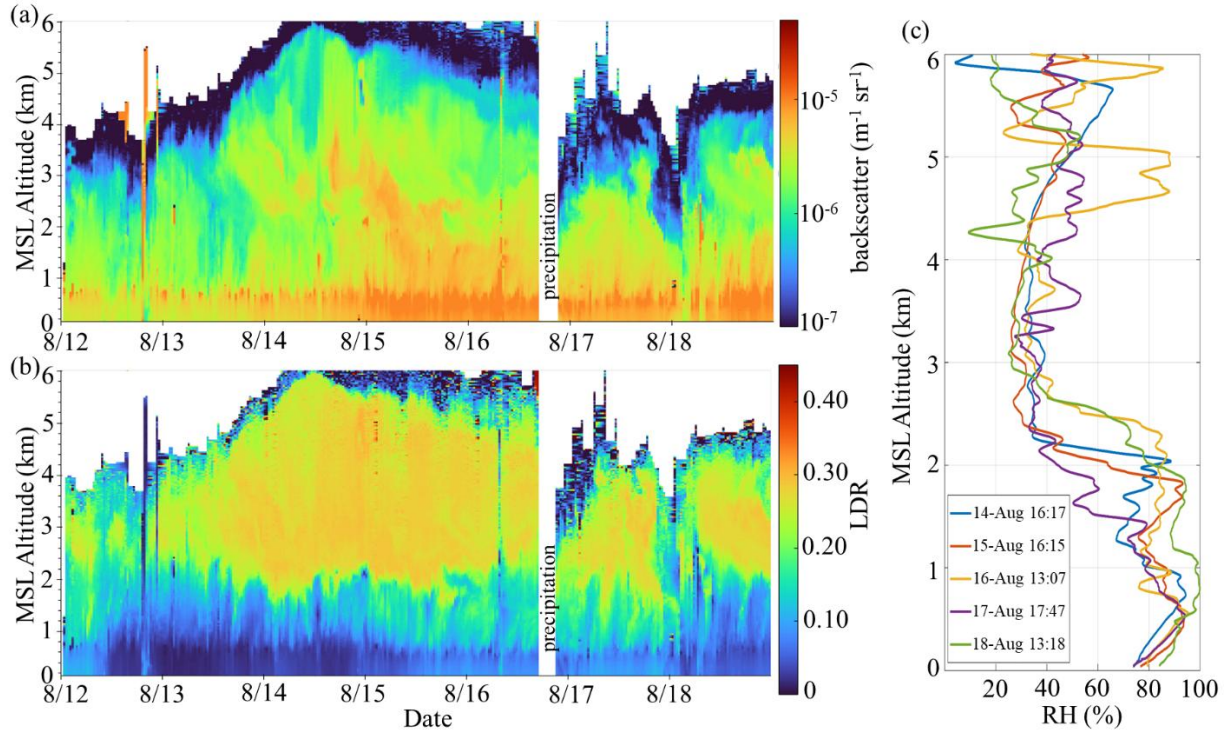
Figure 3. HSRL -measurements for (a) particulate backscatter (m^{-1} sr^{-1}) and (b) particulate linear depolarization ratio (LDR) within 6 km AMSL for August 12 -18, 2023. (c) Vertical profiles of relative humidity (RH, %) up to 6 km AMSL from radiosonde launches at Ragged Point on representative days between August 14 and 18, 2023. In panels (a) and (b), periods with particulate backscatter $<10^{-7}$ (m^{-1} sr^{-1}) are masked out. The uncertainty associated with the particulate LDR measurements shown in panel (b) is provided in Fig. S2.

3.2. Vertical Gradients in the LDR and aerosol mixing state

A vertical gradient in aerosol particle mixing state was observed during the Saharan dust intrusion, wherein dust is internally mixed with sea spray at the surface and externally mixed aloft. Single-particle chemical composition and morphology analysis revealed a diverse set of particle types with distinct chemistries and morphologies, including mineral dust, sea spray, aged sea spray, internally mixed mineral dust and sea spray, sulfates, and organics (Royer et al., 2023;

411   Ault et al., 2012, 2014). The Methods section describes the particle classification approach and

412   the particle types identified in this study. Detailed chemical composition of the particle types is

413   presented in SI Text S2, representative elemental digital color stack plots used for particle

414   classification are shown in Fig. S3, and representative SEM images and corresponding EDX

415   spectra for each particle class are shown in Fig. 4a.

416   Our single particle results from ground-based samples share several similarities with, but

417   also important differences from, previous studies of Saharan dust transported to the Caribbean.

418   Consistent with Harrison et al., 2022; Krejci et al., 2005; Denjean et al., 2015 and Reid et

419   al.,2003a for the Caribbean, the vast majority of dust particles observed at Barbados during

420   MAGPIE were aluminosilicates, confirming the dominance of this mineralogical class in trans-

421   Atlantic Saharan dust. A prominent feature of the MAGPIE observations was the frequent

422   presence of internally mixed dust and sea spray particles, a phenomenon also documented in

423   earlier Caribbean studies (e.g., Reid et al., 2003a; Aryasree et al., 2024; Royer et al., 2025).

424   Kandler et al. (2018) suggested that such mixing likely occurs locally through turbulent

425   interactions between dust and marine aerosol in the MABL. Our observations are consistent with

426   this mechanism and further suggest that cloud processing may enhance this internal mixing.

427   Similar internally mixed dust and sea spray particles have been reported in other coastal regions,

428   particularly during Asian dust outbreaks (Zhang and Iwasaka, 2004; Zhang et al., 2006; Zhang

429   and Iwasaka, 2001; Zhang et al., 2003), indicating that this mixing process is not unique to the

430   Caribbean but may be characteristic of dust outflows across humid marine environments.

431   Figures 4c and S4 present the average size-resolved chemical composition of ground-

432   level aerosol samples collected during the dust event. A clear compositional shift is observed

433   between submicron and super-micron particles. In the submicron range (particle diameter <

434   1 μm), organic and sulfate aerosol particles were dominant, with median diameters of 0.45 μm

435   and 0.36 μm, respectively. In contrast, the super-micron size range was dominated by sea spray,

436   mineral dust, and internally mixed dust and sea spray particles. Externally mixed mineral dust

437   collected through our impactor had a number median diameter of ~1.2 μm, while internally

438   mixed dust and sea spray particles exhibited larger median diameters of ~2.0 μm, likely resulting

439   from coagulation and condensation processes occurring during dust descent into the MABL

440   (Kandler et al., 2018). Further, these particles likely become even larger under the high relative

441   humidity (>80 %) conditions of the MABL consistent with hygroscopic growth (Zieger et al.,

442   2017). This morphological evolution in internally mixed dust and sea salt particles would

443   explain, in part, the suppressed LDR during the major dust intrusion event (Bi et al., 2022).

444
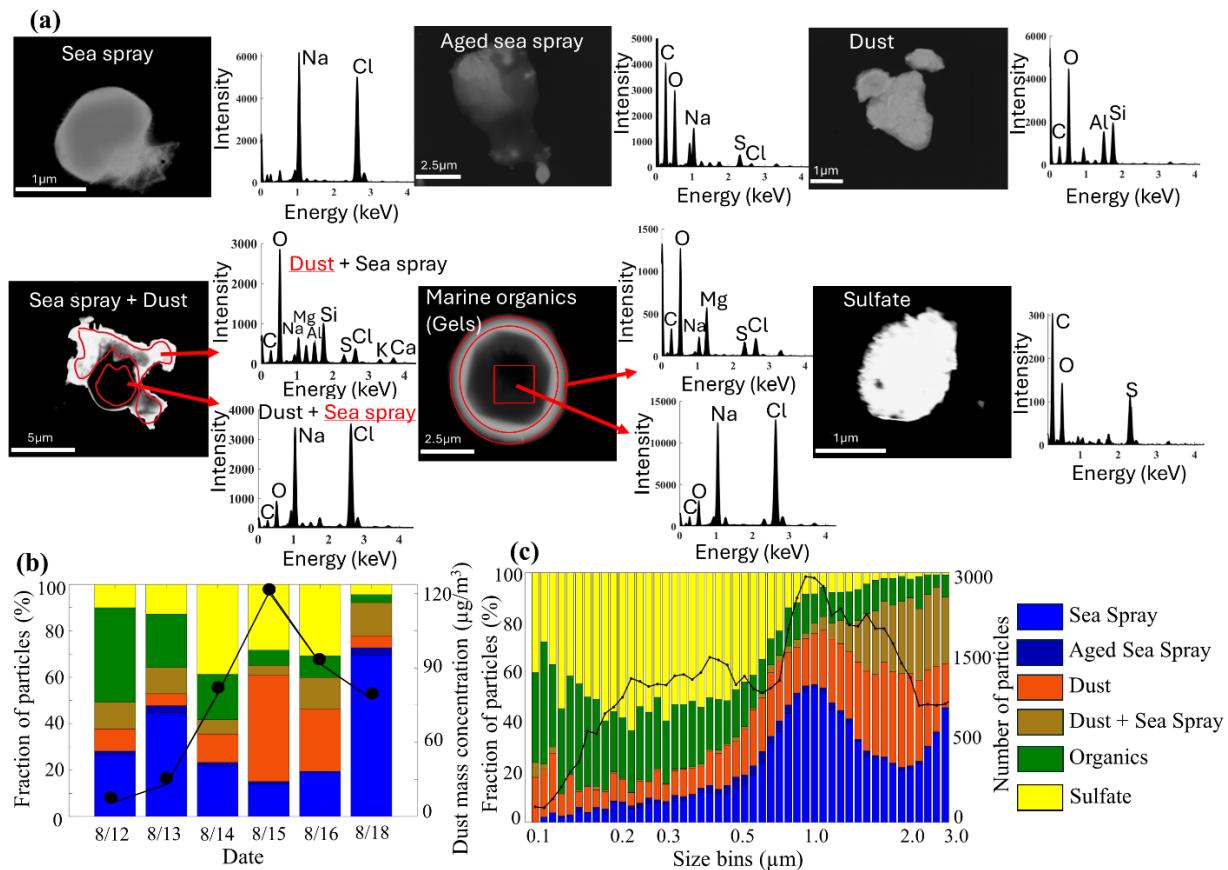
445   Figure 4. (a) Representative aerosol particle types observed in surface samples by SEM images

446   (left) and EDX spectra (right) in samples collected during the MAGPIE campaign. (b) Temporal

447   variations in the number fraction of different particle types during the dust event. (c) Number

448   fractions of different particle types plotted as a function of the particle projected area diameter.

449   The black colored line graph in panels (b) & (c) represents dust mass concentration and number

450   of particles, respectively. These plots are generated from the single particle CCSEM/EDX

451   analysis of the in-situ samples collected at the top of the 17 m tower at BACO.

452   To extend this analysis vertically and examine how particle composition varies with

453   altitude, Fig. 5 presents the vertical profile of the number fractions of aerosol particle types,

454   averaged over the samples taken during dusty days, and HSRL data from August 15 (15:00

455   UTC), the day when Barbados experienced the highest ground-level dust concentration (~120

456   µg/m^3). The SAL was predominantly composed of mineral dust particles (90% of the analyzed

457   particles) transported from Northern Africa, and the LDR observed within the SAL (0.30) is

458   attributable to the large fraction of mineral dust present in this layer. Additionally, a transition

459   layer between the SAL and the MABL (labeled as "Mixture" in Fig. 5b) is shown where both sea

460   salt and mineral dust are concurrently present. In the SAL, a fraction of the dust is internally

461   mixed with sea spray particles (10% of the analyzed particles). Below the SAL, between 0.7 km

462   and 1.8 km, LDR values were much smaller and ranged from 0.10 to 0.20, typical for aerosol

463   regimes within the humid MABL where mineral dust particles are mixed with sea spray particles

464   (Gasteiger et al., 2017; Tesche et al., 2011). A comparison of particle composition across

465   altitudes reveals that samples collected above the cloud top contained a slightly higher number

466   fraction of mineral dust (57%) compared to internally mixed dust and sea spray particles (43%).

467   In contrast, below the cloud base, this ratio was reversed, with internally mixed dust and sea

468   spray particles making up 58% of the dust and externally mixed dust 42% of the dust particles

469   suggesting a dynamic, vertical exchange of particles within the MABL. The MABL circulation

470   pattern through clouds is well documented by lidar observations (e.g., from early studies (Kunkel

471   et al., 1977) to more recent work (Reid et al., 2025). Such cloud processing mechanisms likely

472   enhance coagulation while turbulent updrafts promote collisions between sea spray and dust

473   particles (Matsuki et al., 2010). The presence of a substantial fraction of internally mixed dust

474   and sea spray particles above and below cloud base is expected, given that sea salt is a dominant

475   contributor to cloud droplets (Crosbie et al., 2022). The number fraction of mineral dust particles

476   increased substantially in the MABL during periods of intense dust intrusion, with a distinct peak

477   observed on August 15 (Fig. 4b). However, particle composition was more variable at the surface

478   compared to aloft, consistent with the proximity to the ocean increasing the presence of marine

479   aerosol particles including sea salts, organics, and sulfates (Fig. 5c). Further, at altitudes below

480   0.7 km, LDR values were consistently at or below 0.10, commonly taken as being indicative of

481   the dominance of sea spray particles with reduced dust influence (e.g., "Dusty Marine" in the

482   CALIPSO retrievals; Kim et al., 2018).
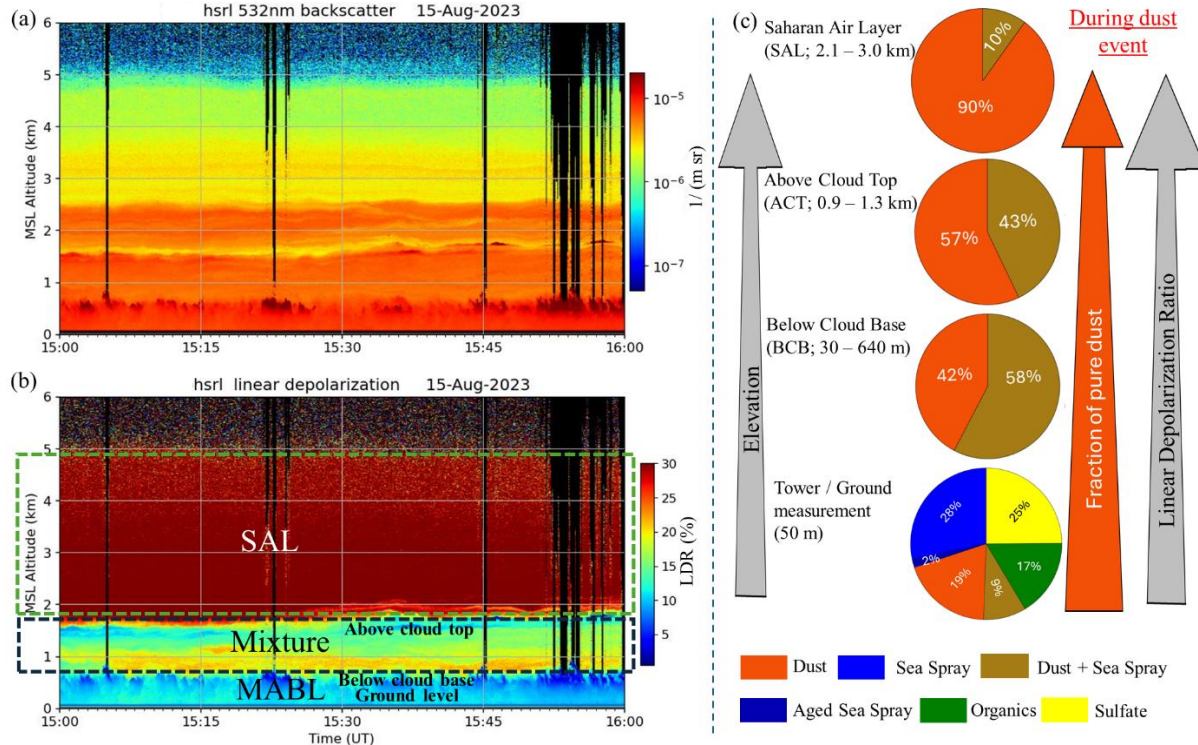
Figure 5. HSRL scan for (a) particulate backscatter at 532 nm and (b) particulate linear

depolarization ratio within 6 km AMSL for August 15, 2023 (15:00 hrs UTC). (c) Pie charts

showing the number concentration (as a percent) of particle types detected from single particle

analysis at different altitudes: SAL, above cloud top, below cloud top, and ground-based samples

collected atop the BACO tower during the dust event. The altitude range where samples

collected for single particle analysis were taken are indicated in parentheses next to each

corresponding pie chart. Pie charts show that with increased elevation, the fraction of externally

mixed dust increased and the linear depolarization ratio (LDR) from the HSRL measurement

increased during the dust event. The RH vertical profile from a radiosonde launched during this

HSRL observation period shown in panels (a) and (b) is shown as the orange line in Fig. 3c.

3.3. Accounting for Dust Mixing State and Hygroscopic Growth in Predicting the LDR

495   Prior work by Denjean et al. (2015) showed that externally mixed African dust did not

496   exhibit hygroscopic growth even at high RH (up to 95%), whereas appreciable water uptake

497   occurs primarily when dust is internally mixed with sea spray, a particle type that was

498   prominently observed in our single-particle analysis. Thus, we evaluated how the expected LDR

499   changes when RH-dependent optical weighting is explicitly accounted for by applying a

500   hygroscopic extinction enhancement factor to internally mixed dust and sea spray particles. The

501   detailed discussion of this hygroscopicity dependent calculation is provided in the SI Text S4,

502   and the resulting LDR predictions are shown in Fig. 6. The enhancement factor (χ) represents the

503   marine aerosol extinction enhancement due to the increase in the marine particle cross-sectional

504   area with increasing RH (i.e., hydroscopic growth) (Hänel, 1972, 1976). When this enhancement

505   factor is included, the estimated LDR is further suppressed, consistent with our observations that

506   dust in the moist MABL becomes internally mixed and more spherical when hydrated. This

507   refined estimate improves closure between the measured and predicted depolarization ratios

508   suggesting that hygroscopic growth of internally mixed dust and sea spray particles play a central

509   role in reducing the lidar depolarization signal. Further, simulations of light scattering by

510   nonspherical particles and coated particle systems by Bi et al. (2022) showed that mineral dust

511   particles coated by a hydrated, low refractive index shell (e.g., water, sulfate, or sea salt) can

512   exhibit a strongly suppressed depolarization signal, often approaching values characteristic of

513   spherical particles. This occurs because at high RH the hygroscopic shell grows substantially and

514   dominates the optical response, effectively masking the non-sphericity of the underlying dust

515   core. This coated particle behavior could provide a physical basis for our observations in the

516   humid MABL, where internally mixed dust and sea spray particles observed at RH consistently

517   exceeding 80% produce low LDR values (<0.1) despite high dust mass concentrations and

518   highlights the need to investigate the role of particle composition and mixing state in modulating

519   depolarization signals. Overall, these observations suggest that the reduced LDR values in the

520   MABL are likely explained, in part, by internally mixed dust and hydrated sea spray particles in

521   the presence of high humidity, resulting in hydrated, more spherical and hence less depolarizing

522   particles.
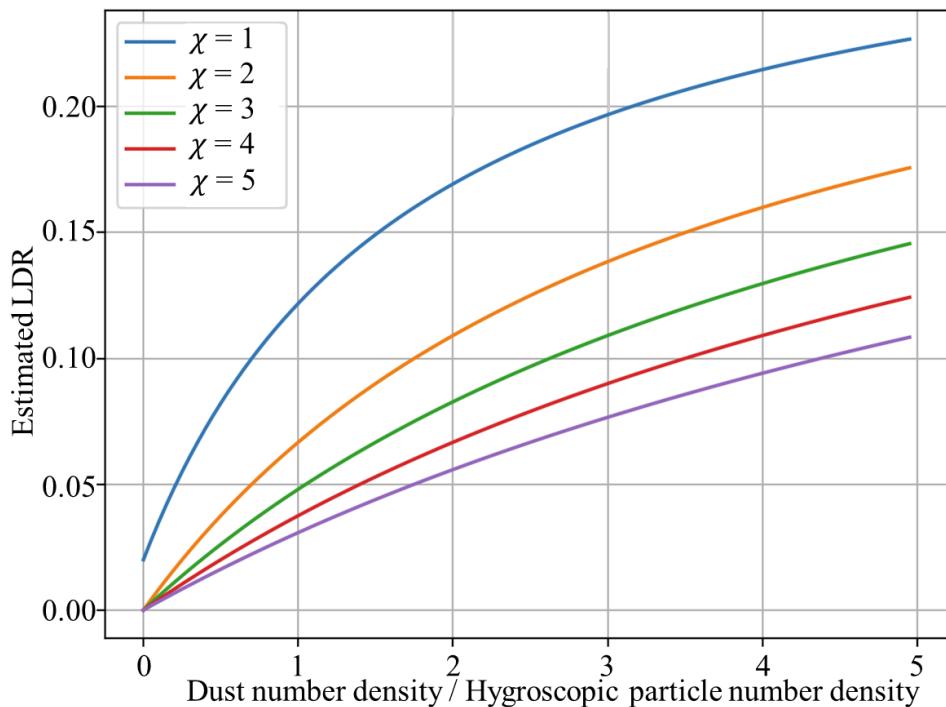
523

524   Figure 6. Relationship between estimated LDR and dust-to-hygroscopic particle number density

525   ratio as a function of marine aerosol extinction enhancement factor (χ) due to hygroscopic

526   growth. The estimates are based on the observed HSRL-LDR for dry dust particles as 0.3 and LR

527   for dry dust particles as 35 sr and the observed average ratio of cross-sectional area of internally

528   mixed dust and sea spray particles to that of externally mixed dust particles as 2.7, derived from

529   CCSEM/EDX single-particle analysis of surface samples collected at BACO. Cross-sectional

530   areas were calculated using the respective median diameters measured for each particle type.

531

4. Conclusions and Atmospheric Implications

Single-particle analysis conducted during the MAGPIE campaign revealed that Saharan dust particles in the MABL are physically and chemically distinct from dust within the SAL aloft. Our results show that in the lower, humid MABL, dust becomes internally mixed with sea spray resulting in potentially enhanced hygroscopicity compared to externally mixed dust in agreement with prior studies investigating the hygroscopicity of transported African dust (Denjean et al., 2015). These changes, in part, suppress the dust's depolarization (being more spherical) signal and complicate its identification by lidar. Despite peak dust loading at BACO (AOD ~0.75; surface dust ~120 µg/m³), HSRL observations showed that LDR values in the lower MABL remained mostly below 0.10, a range typically associated with spherical marine aerosols, even though dust concentrations were ~4.8 times higher than sea salt. This discrepancy is further explained by differences in the scattering (lidar ratio) of dust and marine aerosols, where dust backscatters half the energy per extinction cross-section (lidar ratio) compared to marine aerosols which lowers the depolarization measurement. These combined effects of morphological transformation and different lidar ratios reduce the dust signature in depolarization-based retrievals, complicating its detection and quantification near the surface. The resulting underestimation of surface-level dust by lidar-based depolarization retrievals is of particular concern especially during high-dust events like the one observed during this study, where surface particulate matter (PM) exceeded WHO guidelines for PM_{10} of 45 µg/m^3 (World Health Organization, 2021) by a factor of nearly three. Moreover, it may help explain similar discrepancies between lidar observations and in situ measurements in other regions where dust is modified through interactions with marine aerosols.

554   More broadly, these results highlight the importance of integrating vertically resolved

555   lidar data with in-situ single-particle analysis and surface aerosol mass concentrations to improve

556   the interpretation of lidar observations in dust-affected regions. Such integrated approaches are

557   essential because LDR is widely used in satellite retrieval algorithms and atmospheric models to

558   estimate dust volume and mass fractions, calculate dust-related radiative forcing, estimate dust

559   contribution to cloud condensation and ice nucleation profiles, estimate dust deposition to

560   receptor ecosystems, and predict surface air quality (Meloni et al., 2018; Haarig et al., 2017;

561   Müller et al., 2010, 2012; Yang et al., 2012; Marinou et al., 2017; Proestakis et al., 2018; Adebiyi

562   et al., 2023; Mahowald et al., 2005). Without such integrated observations, satellite retrievals and

563   forecasting systems may significantly underestimate dust impacts near the surface, where they

564   matter most for air quality and biogeochemical feedback.

565   While our results demonstrate that single wavelength depolarization can underestimate

566   near surface dust under humid, mixed aerosol conditions, we emphasize that more advanced

567   remote sensing approaches can mitigate these limitations. Multi-wavelength HSRL observations,

568   including backscatter at 532, and 1064 nm and corresponding color ratio and depolarization

569   metrics, provide additional degrees of freedom for discriminating dust from hydrated marine

570   aerosol particles. In fact, recent upgrades by the SSEC HSRL team have produced the first

571   calibrated 1064 nm HSRL system, that is aimed at being deployed in future studies. These multi-

572   spectral measurements would enable color ratio signatures characteristic of dust to be detected

573   even when LDR is low, thereby providing a remote sensing pathway to constrain surface dust

574   loading. Validating these multi-spectral retrievals requires independent constraints on aerosol

575   composition and morphology. The vertically resolved single particle measurements presented

576   here provide validation of how dust properties change as they mix with sea spray. Thus, rather

than diminishing the utility of lidar, our results highlight the importance of integrating advanced

multi-wavelength lidar products with targeted in-situ observations to improve the accuracy of

surface dust estimates in marine environments.

Data Availability

Dust and sea salt mass concentration data and number counts of particle types detected by

CCSEM/EDX is publicly available in the University of Miami data repository

(https://doi.org/10.17604/1427-0558).

The HSRL data can be accessed through the University of Wisconsin-Madison SSEC repository

at https://hsrl.ssec.wisc.edu/by_site/37/bscat/2025/04/.

The NASA AERONET data can be accessed through https://aeronet.gsfc.nasa.gov.

Author Contribution

Conceptualization of this work was done by SS, RJH, JSR, and CJG. JSR posed the initial

hypothesis and designed the data collection strategy. Collection of samples was conducted by SS,

WJM, ZB, IR, EE, JSR, EB, ADO, RCL, AA, DB, EAR, JRP, AB, RY, QW, TE, EL, MLP, and

CJG, while analysis was done by SS, HEE, NNL, ZC, SC, and RA. The development of method

used in this work was done by SS, REH, WJM, EE, JSR, and CJG. Instrumentation used to

conduct this work was provided by REH, SC, MLP, and CJG. Formal analysis of data was

performed by SS, WJM, and JSR. EE performed the optical calculations of expected LDR.

Validation of data products was performed by SS, RJH, WJM, JSR, AA, and CJG. Data

visualization was performed by SS. Supervision and project administration duties were done by

RJH, JSR, and CJG. SS wrote the original draft for publication, and all the co-authors reviewed

and edited this work.

Competing Interests

The contact author has declared that none of the authors has any competing interests.

Acknowledgements

Financial Support

References

Adams, A. M., Prospero, J. M., and Zhang, C.: CALIPSO-Derived Three-Dimensional Structure of Aerosol over the Atlantic Basin and Adjacent Continents, J. Clim., 25, 6862–6879, https://doi.org/10.1175/JCLI-D-11-00672.1, 2012.

Adebiyi, A., Kok, J. F., Murray, B. J., Ryder, C. L., Stuut, J.-B. W., Kahn, R. A., Knippertz, P., Formenti, P., Mahowald, N. M., Pérez García-Pando, C., Klose, M., Ansmann, A., Samset, B. H., Ito, A., Balkanski, Y., Di Biagio, C., Romanias, M. N., Huang, Y., and Meng, J.: A review of coarse mineral dust in the Earth system, Aeolian Res., 60, 100849, https://doi.org/10.1016/j.aeolia.2022.100849, 2023.

Andreae, M. O., Charlson, R. J., Bruynseels, F., Storms, H., Van Grieken, R., and Maenhaut, W.: Internal Mixture of Sea Salt, Silicates, and Excess Sulfate in Marine Aerosols, Science (80-.)., 232, 1620–1623, https://doi.org/10.1126/science.232.4758.1620, 1986.

Aryasree, S., Kandler, K., Benker, N., Walser, A., Tipka, A., Dollner, M., Seibert, P., and Weinzierl, B.: Vertical Variability in morphology, chemistry and optical properties of the transported Saharan air layer measured from Cape Verde and the Caribbean, R. Soc. Open Sci., 11, https://doi.org/10.1098/rsos.231433, 2024.

Ault, A. P., Peters, T. M., Sawvel, E. J., Casuccio, G. S., Willis, R. D., Norris, G. A., and Grassian, V. H.: Single-Particle SEM-EDX Analysis of Iron-Containing Coarse Particulate Matter in an Urban Environment: Sources and Distribution of Iron within Cleveland, Ohio, Environ. Sci. Technol., 46, 4331–4339, https://doi.org/10.1021/es204006k, 2012.

Ault, A. P., Guasco, T. L., Ryder, O. S., Baltrusaitis, J., Cuadra-Rodriguez, L. A., Collins, D. B., Ruppel, M. J., Bertram, T. H., Prather, K. A., and Grassian, V. H.: Inside versus Outside: Ion Redistribution in Nitric Acid Reacted Sea Spray Aerosol Particles as Determined by Single Particle Analysis, J. Am. Chem. Soc., 135, 14528–14531, https://doi.org/10.1021/ja407117x, 2013.

Ault, A. P., Guasco, T. L., Baltrusaitis, J., Ryder, O. S., Trueblood, J. V., Collins, D. B., Ruppel, M. J., Cuadra-Rodriguez, L. A., Prather, K. A., and Grassian, V. H.: Heterogeneous Reactivity of Nitric Acid with Nascent Sea Spray Aerosol: Large Differences Observed between and within Individual Particles, J. Phys. Chem. Lett., 5, 2493–2500, https://doi.org/10.1021/jz5008802, 2014.

Barkley, A. E., Olson, N. E., Prospero, J. M., Gatineau, A., Panechou, K., Maynard, N. G., Blackwelder, P., China, S., Ault, A. P., and Gaston, C. J.: Atmospheric Transport of North African Dust-Bearing Supermicron Freshwater Diatoms to South America: Implications for Iron Transport to the Equatorial North Atlantic Ocean, Geophys. Res. Lett., 48, https://doi.org/10.1029/2020GL090476, 2021.

Betzer, P. R., Carder, K. L., Duce, R. A., Merrill, J. T., Tindale, N. W., Uematsu, M., Costello, D. K., Young, R. W., Feely, R. A., Breland, J. A., Bernstein, R. E., and Greco, A. M.: Long–range transport of giant mineral aerosol particles, Nature, 336, 568–571, https://doi.org/10.1038/336568a0, 1988.

Bi, L., Wang, Z., Han, W., Li, W., and Zhang, X.: Computation of Optical Properties of Core-Shell Super-Spheroids Using a GPU Implementation of the Invariant Imbedding T-Matrix Method, Front. Remote Sens., 3, https://doi.org/10.3389/frsen.2022.903312, 2022.

Bondy, A. L., Bonanno, D., Moffet, R. C., Wang, B., Laskin, A., and Ault, A. P.: The diverse chemical mixing state of aerosol particles in the southeastern United States, Atmos. Chem. Phys., 18, 12595–12612, https://doi.org/10.5194/acp-18-12595-2018, 2018.

Burton, S. P., Ferrare, R. A., Hostetler, C. A., Hair, J. W., Rogers, R. R., Obland, M. D., Butler,

C. F., Cook, A. L., Harper, D. B., and Froyd, K. D.: Aerosol classification using airborne High Spectral Resolution Lidar measurements – methodology and examples, Atmos. Meas. Tech., 5, 73–98, https://doi.org/10.5194/amt-5-73-2012, 2012.

Burton, S. P., Hair, J. W., Kahnert, M., Ferrare, R. A., Hostetler, C. A., Cook, A. L., Harper, D. B., Berkoff, T. A., Seaman, S. T., Collins, J. E., Fenn, M. A., and Rogers, R. R.: Observations of the spectral dependence of linear particle depolarization ratio of aerosols using NASA Langley airborne High Spectral Resolution Lidar, Atmos. Chem. Phys., 15, 13453–13473, https://doi.org/10.5194/acp-15-13453-2015, 2015.

Carlson, T. N. and Prospero, J. M.: The Large-Scale Movement of Saharan Air Outbreaks over the Northern Equatorial Atlantic, J. Appl. Meteorol. Clim., 11, 283–297, https://doi.org/https://doi.org/10.1175/1520-0450(1972)011< 0283:TLSMOS>2.0.CO;2, 1972.

Casuccio, G. S., Janocko, P. B., Lee, R. J., Kelly, J. F., Dattner, S. L., and Mgebroff, J. S.: The Use of Computer Controlled Scanning Electron Microscopy in Environmental Studies, J. Air Pollut. Control Assoc., 33, 937–943, https://doi.org/10.1080/00022470.1983.10465674, 1983.

Chin, W.-C., Orellana, M. V., and Verdugo, P.: Spontaneous assembly of marine dissolved organic matter into polymer gels, Nature, 391, 568–572, https://doi.org/10.1038/35345, 1998.

Crosbie, E., Ziemba, L. D., Shook, M. A., Robinson, C. E., Winstead, E. L., Thornhill, K. L., Braun, R. A., MacDonald, A. B., Stahl, C., Sorooshian, A., van den Heever, S. C., DiGangi, J. P., Diskin, G. S., Woods, S., Bañaga, P., Brown, M. D., Gallo, F., Hilario, M. R. A., Jordan, C. E., Leung, G. R., Moore, R. H., Sanchez, K. J., Shingler, T. J., and Wiggins, E. B.: Measurement report: Closure analysis of aerosol–cloud composition in tropical maritime warm convection, Atmos. Chem. Phys., 22, 13269–13302, https://doi.org/10.5194/acp-22-13269-2022, 2022.

Denjean, C., Caquineau, S., Desboeufs, K., Laurent, B., Maille, M., Quiñones Rosado, M., Vallejo, P., Mayol-Bracero, O. L., and Formenti, P.: Long-range transport across the Atlantic in summertime does not enhance the hygroscopicity of African mineral dust, Geophys. Res. Lett., 42, 7835–7843, https://doi.org/10.1002/2015GL065693, 2015.

Elliott, H. E., Popendorf, K. J., Blades, E., Royer, H. M., Pollier, C. G. L., Oehlert, A. M., Kukkadapu, R., Ault, A., and Gaston, C. J.: Godzilla mineral dust and La Soufrière volcanic ash fallout immediately stimulate marine microbial phosphate uptake, Front. Mar. Sci., 10, https://doi.org/10.3389/fmars.2023.1308689, 2024.

Eloranta, E. W., Razenkov, I. A., Hedrick, J., and Garcia, J. P.: The design and construction of an airborne high spectral resolution lidar, in: IEEE Aerospace Conference Proceedings, https://doi.org/10.1109/AERO.2008.4526390, 2008.

Freudenthaler, V., Esselborn, M., Wiegner, M., Heese, B., Tesche, M., Ansmann, A., Müller, D., Althausen, D., Wirth, M., Fix, A., Ehret, G., Knippertz, P., Toledano, C., Gasteiger, J., Garhammer, M., and Seefeldner, M.: Depolarization ratio profiling at several wavelengths in pure Saharan dust during SAMUM 2006, Tellus B Chem. Phys. Meteorol., 61, 165, https://doi.org/10.1111/j.1600-0889.2008.00396.x, 2009.

Gasteiger, J., Groß, S., Sauer, D., Haarig, M., Ansmann, A., and Weinzierl, B.: Particle settling and vertical mixing in the Saharan Air Layer as seen from an integrated model, lidar, and in situ perspective, Atmos. Chem. Phys., 17, 297–311, https://doi.org/10.5194/acp-17-297-2017, 2017.

Gaston, C. J., Furutani, H., Guazzotti, S. A., Coffee, K. R., Bates, T. S., Quinn, P. K., Aluwihare,

L. I., Mitchell, B. G., and Prather, K. A.: Unique ocean-derived particles serve as a proxy for changes in ocean chemistry, J. Geophys. Res., 116, D18310, https://doi.org/10.1029/2010JD015289, 2011.

Gaston, C. J., Prospero, J. M., Foley, K., Pye, H. O. T., Custals, L., Blades, E., Sealy, P., and Christie, J. A.: Diverging trends in aerosol sulfate and nitrate measured in the remote North Atlantic in Barbados are attributed to clean air policies, African smoke, and anthropogenic emissions, Atmos. Chem. Phys., 24, 8049–8066, https://doi.org/10.5194/acp-24-8049-2024, 2024.

Giles, D. M., Sinyuk, A., Sorokin, M. G., Schafer, J. S., Smirnov, A., Slutsker, I., Eck, T. F., Holben, B. N., Lewis, J. R., Campbell, J. R., Welton, E. J., Korkin, S. V., and Lyapustin, A. I.: Advancements in the Aerosol Robotic Network (AERONET) Version 3 database – automated near-real-time quality control algorithm with improved cloud screening for Sun photometer aerosol optical depth (AOD) measurements, Atmos. Meas. Tech., 12, 169–209, https://doi.org/10.5194/amt-12-169-2019, 2019.

Groß, S., Freudenthaler, V., Schepanski, K., Toledano, C., Schäfler, A., Ansmann, A., and Weinzierl, B.: Optical properties of long-range transported Saharan dust over Barbados as measured by dual-wavelength depolarization Raman lidar measurements, Atmos. Chem. Phys., 15, 11067–11080, https://doi.org/10.5194/acp-15-11067-2015, 2015.

Groß, S., Gasteiger, J., Freudenthaler, V., Müller, T., Sauer, D., Toledano, C., and Ansmann, A.: Saharan dust contribution to the Caribbean summertime boundary layer – a lidar study during SALTRACE, Atmos. Chem. Phys., 16, 11535–11546, https://doi.org/10.5194/acp-16-11535-2016, 2016.

Haarig, M., Ansmann, A., Althausen, D., Klepel, A., Groß, S., Freudenthaler, V., Toledano, C., Mamouri, R.-E., Farrell, D. A., Prescod, D. A., Marinou, E., Burton, S. P., Gasteiger, J., Engelmann, R., and Baars, H.: Triple-wavelength depolarization-ratio profiling of Saharan dust over Barbados during SALTRACE in 2013 and 2014, Atmos. Chem. Phys., 17, 10767–10794, https://doi.org/10.5194/acp-17-10767-2017, 2017.

Hand, V. L., Capes, G., Vaughan, D. J., Formenti, P., Haywood, J. M., and Coe, H.: Evidence of internal mixing of African dust and biomass burning particles by individual particle analysis using electron beam techniques, J. Geophys. Res. Atmos., 115, https://doi.org/10.1029/2009JD012938, 2010.

Hänel, G.: Computation of the extinction of visible radiation by atmospheric aerosol particles as a function of the relative humidity, based upon measured properties, J. Aerosol Sci., 3, 377–386, https://doi.org/10.1016/0021-8502(72)90092-4, 1972.

Hänel, G.: The Single-Scattering Albedo of Atmospheric Aerosol Particles as a Function of Relative Humidity, J. Atmos. Sci., 33, 1120–1124, https://doi.org/10.1175/1520-0469(1976)033<1120:TSSAOA>2.0.CO;2, 1976.

Harrison, A. D., O'Sullivan, D., Adams, M. P., Porter, G. C. E., Blades, E., Brathwaite, C., Chewitt-Lucas, R., Gaston, C., Hawker, R., Krüger, O. O., Neve, L., Pöhlker, M. L., Pöhlker, C., Pöschl, U., Sanchez-Marroquin, A., Sealy, A., Sealy, P., Tarn, M. D., Whitehall, S., McQuaid, J. B., Carslaw, K. S., Prospero, J. M., and Murray, B. J.: The ice-nucleating activity of African mineral dust in the Caribbean boundary layer, Atmos. Chem. Phys., 22, 9663–9680, https://doi.org/10.5194/acp-22-9663-2022, 2022.

Hayman, M. and Spuler, S.: Demonstration of a diode-laser-based high spectral resolution lidar (HSRL) for quantitative profiling of clouds and aerosols, Opt. Express, 25, A1096, https://doi.org/10.1364/OE.25.0A1096, 2017.

Holben, B. N., Eck, T. F., Slutsker, I., Tanré, D., Buis, J. P., Setzer, A., Vermote, E., Reagan, J. A., Kaufman, Y. J., Nakajima, T., Lavenu, F., Jankowiak, I., and Smirnov, A.: AERONET—A Federated Instrument Network and Data Archive for Aerosol Characterization, Remote Sens. Environ., 66, 1–16, https://doi.org/10.1016/S0034-4257(98)00031-5, 1998.

Huang, X., Yang, P., Kattawar, G., and Liou, K.-N.: Effect of mineral dust aerosol aspect ratio on polarized reflectance, J. Quant. Spectrosc. Radiat. Transf., 151, 97–109, https://doi.org/10.1016/j.jqsrt.2014.09.014, 2015.

Kalashnikova, O. V., Garay, M. J., Martonchik, J. V., and Diner, D. J.: MISR Dark Water aerosol retrievals: operational algorithm sensitivity to particle non-sphericity, Atmos. Meas. Tech., 6, 2131–2154, https://doi.org/10.5194/amt-6-2131-2013, 2013.

Kandler, K., Schneiders, K., Ebert, M., Hartmann, M., Weinbruch, S., Prass, M., and Pöhlker, C.: Composition and mixing state of atmospheric aerosols determined by electron microscopy: method development and application to aged Saharan dust deposition in the Caribbean boundary layer, Atmos. Chem. Phys., 18, 13429–13455, https://doi.org/10.5194/acp-18-13429-2018, 2018.

Karyampudi, V. M. and Carlson, T. N.: Analysis and Numerical Simulations of the Saharan Air Layer and Its Effect on Easterly Wave Disturbances, J. Atmos. Sci., 45, 3102–3136, https://doi.org/10.1175/1520-0469(1988)045<3102:AANSOT>2.0.CO;2, 1988.

Karyampudi, V. M., Palm, S. P., Reagen, J. A., Fang, H., Grant, W. B., Hoff, R. M., Moulin, C., Pierce, H. F., Torres, O., Browell, E. V., and Melfi, S. H.: Validation of the Saharan Dust Plume Conceptual Model Using Lidar, Meteosat, and ECMWF Data, Bull. Am. Meteorol. Soc., 80, 1045–1075, https://doi.org/10.1175/1520-0477(1999)080<1045:VOTSDP>2.0.CO;2, 1999.

Kim, D. S., Hopke, P. K., Massart, D. L., Kaufman, L., and Casuccio, G. S.: Multivariate analysis of CCSEM auto emission data, Sci. Total Environ., 59, 141–155, https://doi.org/10.1016/0048-9697(87)90438-4, 1987.

Kim, M.-H., Omar, A. H., Tackett, J. L., Vaughan, M. A., Winker, D. M., Trepte, C. R., Hu, Y., Liu, Z., Poole, L. R., Pitts, M. C., Kar, J., and Magill, B. E.: The CALIPSO version 4 automated aerosol classification and lidar ratio selection algorithm, Atmos. Meas. Tech., 11, 6107–6135, https://doi.org/10.5194/amt-11-6107-2018, 2018.

Koehler, K. A., Kreidenweis, S. M., DeMott, P. J., Prenni, A. J., and Petters, M. D.: Potential impact of Owens (dry) Lake dust on warm and cold cloud formation, J. Geophys. Res. Atmos., 112, https://doi.org/10.1029/2007JD008413, 2007.

Kong, S., Sato, K., and Bi, L.: Lidar Ratio–Depolarization Ratio Relations of Atmospheric Dust Aerosols: The Super-Spheroid Model and High Spectral Resolution Lidar Observations, J. Geophys. Res. Atmos., 127, https://doi.org/10.1029/2021JD035629, 2022.

Krejci, R., Ström, J., de Reus, M., and Sahle, W.: Single particle analysis of the accumulation mode aerosol over the northeast Amazonian tropical rain forest, Surinam, South America, Atmos. Chem. Phys., 5, 3331–3344, https://doi.org/10.5194/acp-5-3331-2005, 2005.

Krueger, B. J., Grassian, V. H., Cowin, J. P., and Laskin, A.: Heterogeneous chemistry of

790 individual mineral dust particles from different dust source regions: the importance of particle
791 mineralogy, Atmos. Environ., 38, 6253–6261, https://doi.org/10.1016/j.atmosenv.2004.07.010,
792 2004.

793 Kunkel, K. E., Eloranta, E. W., and Shipley, S. T.: Lidar Observations of the Convective
794 Boundary Layer, J. Appl. Meteorol., 16, 1306–1311, https://doi.org/10.1175/1520-
795 0450(1977)016<1306:LOOTCB>2.0.CO;2, 1977.

796 Levin, Z., Teller, A., Ganor, E., and Yin, Y.: On the interactions of mineral dust, sea-salt
797 particles, and clouds: A measurement and modeling study from the Mediterranean Israeli Dust
798 Experiment campaign, J. Geophys. Res. Atmos., 110, https://doi.org/10.1029/2005JD005810,
799 2005.

800 Li-Jones, X., Maring, H. B., and Prospero, J. M.: Effect of relative humidity on light scattering
801 by mineral dust aerosol as measured in the marine boundary layer over the tropical Atlantic
802 Ocean, J. Geophys. Res. Atmos., 103, 31113–31121, https://doi.org/10.1029/98JD01800, 1998.

803 Li, C., Li, J., Dubovik, O., Zeng, Z.-C., and Yung, Y. L.: Impact of Aerosol Vertical Distribution
804 on Aerosol Optical Depth Retrieval from Passive Satellite Sensors, Remote Sens., 12, 1524,
805 https://doi.org/10.3390/rs12091524, 2020.

806 Mahowald, N. M., Baker, A. R., Bergametti, G., Brooks, N., Duce, R. A., Jickells, T. D.,
807 Kubilay, N., Prospero, J. M., and Tegen, I.: Atmospheric global dust cycle and iron inputs to the
808 ocean, Global Biogeochem. Cycles, 19, https://doi.org/10.1029/2004GB002402, 2005.

809 Marinou, E., Amiridis, V., Binietoglou, I., Tsikerdekis, A., Solomos, S., Proestakis, E., Konsta,
810 D., Papagiannopoulos, N., Tsekeri, A., Vlastou, G., Zanis, P., Balis, D., Wandinger, U., and
811 Ansmann, A.: Three-dimensional evolution of Saharan dust transport towards Europe based on a
812 9-year EARLINET-optimized CALIPSO dataset, Atmos. Chem. Phys., 17, 5893–5919,
813 https://doi.org/10.5194/acp-17-5893-2017, 2017.

814 Matsuki, A., Schwarzenboeck, A., Venzac, H., Laj, P., Crumeyrolle, S., and Gomes, L.: Cloud
815 processing of mineral dust: direct comparison of cloud residual and clear sky particles during
816 AMMA aircraft campaign in summer 2006, Atmos. Chem. Phys., 10, 1057–1069,
817 https://doi.org/10.5194/acp-10-1057-2010, 2010.

818 Mayol-Bracero, O. L., Prospero, J. M., Sarangi, B., Andrews, E., Colarco, P. R., Cuevas, E., Di
819 Girolamo, L., Garcia, R. D., Gaston, C., Holben, B., Ladino, L. A., León, P., Losno, R.,
820 Martínez, O., Martínez-Huertas, B. L., Méndez-Lázaro, P., Molinie, J., Muller-Karger, F., Otis,
821 D., Raga, G., Reyes, A., Rosas Nava, J., Rosas, D., Sealy, A., Serikov, I., Tong, D., Torres-
822 Delgado, E., Yu, H., and Zuidema, P.: "Godzilla," the Extreme African Dust Event of June 2020:
823 Origins, Transport, and Impact on Air Quality in the Greater Caribbean Basin, Bull. Am.
824 Meteorol. Soc., 106, E1620–E1648, https://doi.org/10.1175/BAMS-D-24-0045.1, 2025.

825 Mehra, M., Shrestha, S., AP, K., Guagenti, M., Moffett, C. E., VerPloeg, S. G., Coogan, M. A.,
826 Rai, M., Kumar, R., Andrews, E., Sherman, J. P., Flynn III, J. H., Usenko, S., and Sheesley, R.
827 J.: Atmospheric heating in the US from saharan dust: Tracking the June 2020 event with surface
828 and satellite observations, Atmos. Environ., 310, 119988,
829 https://doi.org/10.1016/j.atmosenv.2023.119988, 2023.

830 Meloni, D., di Sarra, A., Brogniez, G., Denjean, C., De Silvestri, L., Di Iorio, T., Formenti, P.,
831 Gómez-Amo, J. L., Gröbner, J., Kouremeti, N., Liuzzi, G., Mallet, M., Pace, G., and Sferlazzo,

D. M.: Determining the infrared radiative effects of Saharan dust: a radiative transfer modelling study based on vertically resolved measurements at Lampedusa, Atmos. Chem. Phys., 18, 4377–4401, https://doi.org/10.5194/acp-18-4377-2018, 2018.

Moustaka, A., Kazadzis, S., Proestakis, E., Lopatin, A., Dubovik, O., Tourpali, K., Zerefos, C., Amiridis, V., and Gkikas, A.: Enhancing dust aerosols monitoring capabilities across North Africa and the Middle East using the A-Train satellite constellation, https://doi.org/10.5194/egusphere-2025-888, 24 March 2025.

Müller, D., Weinzierl, B., Petzold, A., Kandler, K., Ansmann, A., Müller, T., Tesche, M., Freudenthaler, V., Esselborn, M., Heese, B., Althausen, D., Schladitz, A., Otto, S., and Knippertz, P.: Mineral dust observed with AERONET Sun photometer, Raman lidar, and in situ instruments during SAMUM 2006: Shape-independent particle properties, J. Geophys. Res. Atmos., 115, https://doi.org/10.1029/2009JD012520, 2010.

Müller, D., Lee, K. -H., Gasteiger, J., Tesche, M., Weinzierl, B., Kandler, K., Müller, T., Toledano, C., Otto, S., Althausen, D., and Ansmann, A.: Comparison of optical and microphysical properties of pure Saharan mineral dust observed with AERONET Sun photometer, Raman lidar, and in situ instruments during SAMUM 2006, J. Geophys. Res. Atmos., 117, https://doi.org/10.1029/2011JD016825, 2012.

O'Dowd, C. D. and de Leeuw, G.: Marine aerosol production: a review of the current knowledge, Philos. Trans. R. Soc. A Math. Phys. Eng. Sci., 365, 1753–1774, https://doi.org/10.1098/rsta.2007.2043, 2007.

O'Neill, N. T., Eck, T. F., Smirnov, A., Holben, B. N., and Thulasiraman, S.: Spectral discrimination of coarse and fine mode optical depth, J. Geophys. Res. Atmos., 108, https://doi.org/10.1029/2002JD002975, 2003.

Orozco, D., Beyersdorf, A. J., Ziemba, L. D., Berkoff, T., Zhang, Q., Delgado, R., Hennigan, C. J., Thornhill, K. L., Young, D. E., Parworth, C., Kim, H., and Hoff, R. M.: Hygrosopicity measurements of aerosol particles in the San Joaquin Valley, CA, Baltimore, MD, and Golden, CO, J. Geophys. Res. Atmos., 121, 7344–7359, https://doi.org/10.1002/2015JD023971, 2016.

Proestakis, E., Amiridis, V., Marinou, E., Georgoulias, A. K., Solomos, S., Kazadzis, S., Chimot, J., Che, H., Alexandri, G., Binietoglou, I., Daskalopoulou, V., Kourtidis, K. A., de Leeuw, G., and van der A, R. J.: Nine-year spatial and temporal evolution of desert dust aerosols over South and East Asia as revealed by CALIOP, Atmos. Chem. Phys., 18, 1337–1362, https://doi.org/10.5194/acp-18-1337-2018, 2018.

Prospero, J. M.: Mineral and sea salt aerosol concentrations in various ocean regions, J. Geophys. Res. Ocean., 84, 725–731, https://doi.org/10.1029/JC084iC02p00725, 1979.

Prospero, J. M.: Long-term measurements of the transport of African mineral dust to the southeastern United States: Implications for regional air quality, J. Geophys. Res. Atmos., 104, 15917–15927, https://doi.org/10.1029/1999JD900072, 1999.

Prospero, J. M., Delany, A. C., Delany, A. C., and Carlson, T. N.: The Discovery of African Dust Transport to the Western Hemisphere and the Saharan Air Layer: A History, Bull. Am. Meteorol. Soc., 102, E1239–E1260, https://doi.org/10.1175/BAMS-D-19-0309.1, 2021.

Razenkov, I.: Characterization of a Geiger-Mode Avalanche Photodiode Detector for High Special Resolution Lidar, University of Wisconsin - Madison, 2010.

874 Reid, E. A., Reid, J. S., Meier, M. M., Dunlap, M. R., Cliff, S. S., Broumas, A., Perry, K., and
875 Maring, H.: Characterization of African dust transported to Puerto Rico by individual particle
876 and size segregated bulk analysis, J. Geophys. Res. Atmos., 108,
877 https://doi.org/10.1029/2002JD002935, 2003a.

878 Reid, J. S., Jonsson, H. H., Maring, H. B., Smirnov, A., Savoie, D. L., Cliff, S. S., Reid, E. A.,
879 Livingston, J. M., Meier, M. M., Dubovik, O., and Tsay, S.: Comparison of size and
880 morphological measurements of coarse mode dust particles from Africa, J. Geophys. Res.
881 Atmos., 108, https://doi.org/10.1029/2002JD002485, 2003b.

882 Reid, J. S., Holz, R. E., Hostetler, C. A., Ferrare, R. A., Rubin, J. I., Thompson, E. J., van den
883 Heever, S. C., Amiot, C. G., Burton, S. P., DiGangi, J. P., Diskin, G. S., Cossuth, J. H.,
884 Eleuterio, D. P., Eloranta, E. W., Kuehn, R., Marais, W. J., Maring, H. B., Sorooshian, A.,
885 Thornhill, K. L., Trepte, C. R., Wang, J., Xian, P., and Ziemba, L. D.: PISTON and CAMP 2 Ex
886 observations of the fundamental modes of aerosol vertical variability in the Northwest Tropical
887 Pacific and Maritime Continent's Monsoon, https://doi.org/10.5194/egusphere-2025-2605, 12
888 August 2025.

889 Riemer, N., Ault, A. P., West, M., Craig, R. L., and Curtis, J. H.: Aerosol Mixing State:
890 Measurements, Modeling, and Impacts, Rev. Geophys., 57, 187–249,
891 https://doi.org/10.1029/2018RG000615, 2019.

892 Royer, H. M., Pöhlker, M. L., Krüger, O., Blades, E., Sealy, P., Lata, N. N., Cheng, Z., China, S.,
893 Ault, A. P., Quinn, P. K., Zuidema, P., Pöhlker, C., Pöschl, U., Andreae, M., and Gaston, C. J.:
894 African smoke particles act as cloud condensation nuclei in the wintertime tropical North
895 Atlantic boundary layer over Barbados, Atmos. Chem. Phys., 23, 981–998,
896 https://doi.org/10.5194/acp-23-981-2023, 2023.

897 Royer, H. M., Sheridan, M. T., Elliott, H. E., Lata, N. N., Cheng, Z., China, S., Zhu, Z., Ault, A.
898 P., and Gaston, C. J.: African dust transported to Barbados in the Wintertime Lacks Indicators of
899 Chemical Aging, Atmos. Chem. Phys., https://doi.org/10.5194/egusphere-2024-3288, 2025.

900 Scheuvens, D., Schütz, L., Kandler, K., Ebert, M., and Weinbruch, S.: Bulk composition of
901 northern African dust and its source sediments — A compilation, Earth-Science Rev., 116, 170–
902 194, https://doi.org/10.1016/j.earscirev.2012.08.005, 2013.

903 Shen, H., Peters, T. M., Casuccio, G. S., Lersch, T. L., West, R. R., Kumar, A., Kumar, N., and
904 Ault, A. P.: Elevated Concentrations of Lead in Particulate Matter on the Neighborhood-Scale in
905 Delhi, India As Determined by Single Particle Analysis, Environ. Sci. Technol., 50, 4961–4970,
906 https://doi.org/10.1021/acs.est.5b06202, 2016.

907 Stevens, B., Farrell, D., Hirsch, L., Jansen, F., Nuijens, L., Serikov, I., Brügmann, B., Forde, M.,
908 Linne, H., Lonitz, K., and Prospero, J. M.: The Barbados Cloud Observatory: Anchoring
909 Investigations of Clouds and Circulation on the Edge of the ITCZ, Bull. Am. Meteorol. Soc., 97,
910 787–801, https://doi.org/https://doi.org/10.1175/BAMS-D-14-00247.1, 2016.

911 Tesche, M., Müller, D., Gross, S., Ansmann, A., Althausen, D., Freudenthaler, V., Weinzierl, B.,
912 Veira, A., and Petzold, A.: Optical and microphysical properties of smoke over Cape Verde
913 inferred from multiwavelength lidar measurements, Tellus B Chem. Phys. Meteorol., 63, 677,
914 https://doi.org/10.1111/j.1600-0889.2011.00549.x, 2011.

915 Titos, G., Cazorla, A., Zieger, P., Andrews, E., Lyamani, H., Granados-Muñoz, M. J., Olmo, F.

916 J., and Alados-Arboledas, L.: Effect of hygroscopic growth on the aerosol light-scattering
917 coefficient: A review of measurements, techniques and error sources, Atmos. Environ., 141,
918 494–507, https://doi.org/10.1016/j.atmosenv.2016.07.021, 2016.

919 Tsamalis, C., Chédin, A., Pelon, J., and Capelle, V.: The seasonal vertical distribution of the
920 Saharan Air Layer and its modulation by the wind, Atmos. Chem. Phys., 13, 11235–11257,
921 https://doi.org/10.5194/acp-13-11235-2013, 2013.

922 Weinzierl, B., Ansmann, A., Prospero, J. M., Althausen, D., Benker, N., Chouza, F., Dollner, M.,
923 Farrell, D., Fomba, W. K., Freudenthaler, V., Gasteiger, J., Groß, S., Haarig, M., Heinold, B.,
924 Kandler, K., Kristensen, T. B., Mayol-Bracero, O. L., Müller, T., Reitebuch, O., Sauer, D.,
925 Schäfler, A., Schepanski, K., Spanu, A., Tegen, I., Toledano, C., and Walser, A.: The Saharan
926 Aerosol Long-Range Transport and Aerosol–Cloud-Interaction Experiment: Overview and
927 Selected Highlights, Bull. Am. Meteorol. Soc., 98, 1427–1451, https://doi.org/10.1175/BAMS-
928 D-15-00142.1, 2017.

929 Winkler, P.: The growth of atmospheric aerosol particles as a function of the relative humidity—
930 II. An improved concept of mixed nuclei, J. Aerosol Sci., 4, 373–387,
931 https://doi.org/10.1016/0021-8502(73)90027-X, 1973.

932 World Health Organization: WHO global air quality guidlines. Particulate matter (PM2.5 and
933 PM10), ozone, nitrogen dioxide, sulfur dioxide and carbon monoxide, Geneva, 290 pp., 2021.

934 Xian, P., Reid, J. S., Hyer, E. J., Sampson, C. R., Rubin, J. I., Ades, M., Asencio, N., Basart, S.,
935 Benedetti, A., Bhattacharjee, P. S., Brooks, M. E., Colarco, P. R., da Silva, A. M., Eck, T. F.,
936 Guth, J., Jorba, O., Kouznetsov, R., Kipling, Z., Sofiev, M., Perez Garcia-Pando, C., Pradhan,
937 Y., Tanaka, T., Wang, J., Westphal, D. L., Yumimoto, K., and Zhang, J.: Current state of the
938 global operational aerosol multi-model ensemble: An update from the International Cooperative
939 for Aerosol Prediction (ICAP), Q. J. R. Meteorol. Soc., 145, 176–209,
940 https://doi.org/10.1002/qj.3497, 2019.

941 Yang, L., Zhang, S., Tao, H., Yang, Y., Wang, L., Cui, Y., Xu, Y., and Li, X.: Comprehensive
942 Analysis of a Dust Storm by a Lidar Network Combined With Multiple Data, Front. Environ.
943 Sci., 10, https://doi.org/10.3389/fenvs.2022.832710, 2022.

944 Yang, W., Marshak, A., Várnai, T., Kalashnikova, O. V., and Kostinski, A. B.: CALIPSO
945 observations of transatlantic dust: vertical stratification and effect of clouds, Atmos. Chem.
946 Phys., 12, 11339–11354, https://doi.org/10.5194/acp-12-11339-2012, 2012.

947 Zhang, D. and Iwasaka, Y.: Chlorine deposition on dust particles in marine atmosphere,
948 Geophys. Res. Lett., 28, 3613–3616, https://doi.org/10.1029/2001GL013333, 2001.

949 Zhang, D. and Iwasaka, Y.: Size change of Asian dust particles caused by sea salt interaction:
950 Measurements in southwestern Japan, Geophys. Res. Lett., 31,
951 https://doi.org/10.1029/2004GL020087, 2004.

952 Zhang, D., Zang, J., Shi, G., Iwasaka, Y., Matsuki, A., and Trochkine, D.: Mixture state of
953 individual Asian dust particles at a coastal site of Qingdao, China, Atmos. Environ., 37, 3895–
954 3901, https://doi.org/10.1016/S1352-2310(03)00506-5, 2003.

955 Zhang, D., Iwasaka, Y., Matsuki, A., Ueno, K., and Matsuzaki, T.: Coarse and accumulation
956 mode particles associated with Asian dust in southwestern Japan, Atmos. Environ., 40, 1205–
957 1215, https://doi.org/10.1016/j.atmosenv.2005.10.037, 2006.

958   Zhang, X., Massoli, P., Quinn, P. K., Bates, T. S., and Cappa, C. D.: Hygroscopic growth of
959   submicron and supermicron aerosols in the marine boundary layer, J. Geophys. Res. Atmos.,
960   119, 8384–8399, https://doi.org/10.1002/2013JD021213, 2014.

961   Zieger, P., Väisänen, O., Corbin, J. C., Partridge, D. G., Bastelberger, S., Mousavi-Fard, M.,
962   Rosati, B., Gysel, M., Krieger, U. K., Leck, C., Nenes, A., Riipinen, I., Virtanen, A., and Salter,
963   M. E.: Revising the hygroscopicity of inorganic sea salt particles, Nat. Commun., 8,
964   https://doi.org/doi.org/10.1038/ncomms15883, 2017.

965   Zuidema, P., Alvarez, C., Kramer, S. J., Custals, L., Izaguirre, M., Sealy, P., Prospero, J. M., and
966   Blades, E.: Is Summer African Dust Arriving Earlier to Barbados? The Updated Long-Term In
967   Situ Dust Mass Concentration Time Series from Ragged Point, Barbados, and Miami, Florida,
968   Bull. Am. Meteorol. Soc., 100, 1981–1986, https://doi.org/10.1175/BAMS-D-18-0083.1, 2019.

969